Superfluid Quantum Interference in Multiple-Turn Reciprocal Geometry

Supradeep Narayana and Yuki Sato

Phys. Rev. Lett. **106**, 255301 — Published 20 June 2011

DOI: 10.1103/PhysRevLett.106.255301

Superfluid quantum interference in multiple-turn reciprocal geometry

Supradeep Narayana and Yuki Sato
The Rowland Institute at Harvard, Harvard University, Cambridge, MA 02142
(Dated: May 23, 2011)

We report the observation of superfluid quantum interference in a compact, large area matter-wave interferometer consisting of a multiple-turn interfering path in reciprocal geometry. Utilizing the Sagnac effect from the Earth's rotation in conjunction with a phase shifter made of superfluid heat current, we demonstrate that such a scheme can be extended for sensitive rotation sensing as well as for general interferometry.

PACS numbers: 07.60.Ly, 03.75.-b, 85.25.Dq

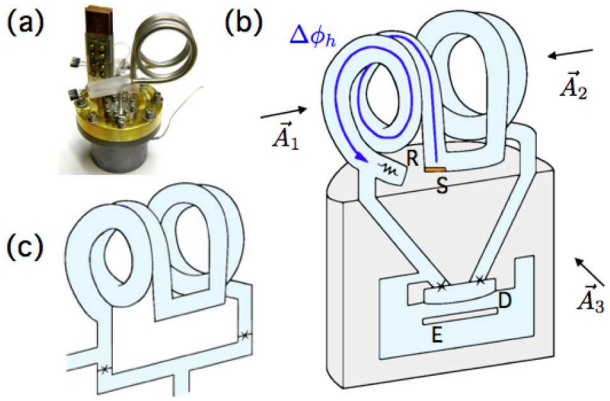

FIG. 1. (a) Experimental apparatus. (b) Schematic representation. The X's indicate the two channel arrays. A flexible metalized diaphragm (D) and a fixed electrode (E) are used to create pressure difference across the nano-channels. The diaphragm also forms the input element for a sensitive microphone based on superconducting electronics (not shown) to detect the mass current oscillation. A heater (R) and a thin Cu sheet (S) connected to the helium bath outside serve as a heat source and a temperature sink for one set of loops. $\Delta\phi_h$ indicates the thermally-driven phase shift. The interference path encloses an area characterized by three area vectors, $\vec{A}_1$, $\vec{A}_2$, and $\vec{A}_3$. The height of the apparatus is ∼9 cm. (c) Simplified view of the interference loop.

In conventional interferometry devices, beams of light [1] or atoms [2] are split and recombined while enclosing an area A. Certain physical interactions give rise to a phase shift between the two beams, with the size of the shift proportional to A and the "mass" of the constituent particles (m for atoms and $\hbar\omega/c^2$ for photons). Because of the larger mass, phase shift for atoms with the same interferometer area is typically 10^{10-11} times larger than it is for visible photons. This makes the matter-wave based interferometer a promising candidate for providing unprecedented sensitivities to external phase shifting influences. For example, when configured as a Sagnac-interferometry-based gyroscope [3], such a device could be used for rotation sensing with possible applications expected in geodesy, seismology, inertial navigation, and potentially testing fundamental theories such as frame-dragging effects [4] predicted by general relativity.

For the precision measurements identified above, interferometer parameters become a compromise between the desire for the best resolution achievable and the reality of the noisy environment. Although increasing the area would improve their sensitivity, interferometers need to be as compact as possible to suppress phase shifts due to environmental noise as well as those due to stray fields. Larger apparatus would also limit the applications of the device. A natural solution to these rather contradictory requirements is to let the interfering path circulate around a small physical area multiple times. One can even envision counter-winding the path in reciprocal geometry. Such a system would allow common rejection of phase shifts due to static perturbations, essentially making the device a 1^{st}-order gradiometer [5].

Some of these techniques have been explored with high finesse mirrors in ring-laser interferometers [6] and with multiple fiber turns in fiber-optic gyroscopes [7]. Although this past decade has seen dramatic progress in researchers' ability to coherently manipulate the motion of atoms, these multiple-turn approaches have been challenging for atom interferometers in confined geometry due to large dispersive coupling of motion between the guide and confining directions in curved atomic waveguides [8, 9]. Here we demonstrate a superfluid ^{4}He matter wave interferometer with multiple turns in reciprocal geometry. We show that this type of configuration can be extended for sensitive rotation sensing as well as for general interferometry. Our results also reveal important differences between superfluid-based interferometers and atom and optical interferometers as well as superconducting quantum interference devices.

A picture of our apparatus is shown in Fig 1(a) and is schematically represented in Fig 1(b). A small volume is bounded on one side by two arrays of nanoscale channels and the other side by a flexible diaphragm. Each array consists of 5,625 channels spaced on 2 μm square lattice in a 60nm-thick silicon nitride membrane. Flow measurements above the superfluid transition temperature T_λ indicate that the channels are 45 ± 7 nm in diameter. The inside is filled with superfluid ^{4}He, and we configure the apparatus to form a loop of superfluid interrupted by two weak link junctions. See Fig 1(c).

In an ideal weak coupling limit, the mass current across the channel arrays is governed by the Josephson current-phase relation $I = I_0 sin\Delta\phi$, where I_0 is the critical current and $\Delta\phi$ is the quantum phase difference across the junction [10]. In operation, we apply a chemical potential difference $\Delta\mu$ (combining pressure and temperature differences) across

the pair of channel arrays. Fluid within each array exhibits mass current oscillation [11, 12] at a Josephson frequency $\Delta\mu/h$. The combined oscillation amplitude from two arrays exhibits interference depending on the external phase shift $\Delta\phi_{ext}$ injected into the system. In a general case where each array exhibits different oscillation amplitudes I_1 and I_2, the overall amplitude can be written as $(I_1+I_2)\sqrt{cos^2(\Delta\phi_{ext}/2)+\gamma^2 sin^2(\Delta\phi_{ext}/2)}$, where $\gamma \equiv (I_1-I_2)/(I_1+I_2)$ is the asymmetry factor. We measure this amplitude by taking a fast Fourier transform of the Josephson current oscillations.

Phase shift $\Delta\phi_{ext}$ can be induced in variety of ways. Rotation-induced phase shift has been studied extensively using light [1], neutrons [13], neutral atoms [3, 14–16] and electrons [17]. Such phase shift based on the Sagnac effect is given by $\Delta\phi_s = (2m_4/\hbar)\vec{\Omega}\cdot\vec{A}$, and through this relation, the interferometer constitutes a gyroscope that responds to the slightest deviation of its frame from an inertial frame.

Since superfluid velocity is fundamentally related to quantum mechanical phase gradient by $v_s = (\hbar/m_4) \bigtriangledown \phi$, one can also inject phase bias along an interferometer loop by locally creating thermally driven superfluid current. Such phase shift is given by $\Delta\phi_h = (m_4/\hbar)(l/\sigma)(\rho_n/\rho\rho_s sT)\dot{Q}$, where ρ, ρ_n, and ρ_s are the total, normal, and superfluid densities, s is the entropy per unit mass, T is the temperature, and σ and l are the cross-sectional area and the length of the heat current pipe [18].

We distinguish superfluid quantum interference devices from other interferometers in which collective effects are not significant. Single atom interferometers or even atoms launched from magneto-optical traps are typically not dense enough to exhibit significant nonlinear effects. On the other hand, for a superfluid interferometer, all the atoms are in a single macroscopic entangled state, and the device technology relies on the nonlinear dynamics of Josephson weak links placed in a loop governed by a macroscopic wavefunction. A superfluid interferometer is a neutral analogue of a dc superconducting quantum interference device (dc-SQUID [19]), where the role of a magnetic field is now played by inertial as well as gauge field rotations [20]. The neutral fluid aspect of the device has some interesting consequences, as will be shown below. We note that an area-enclosing geometry for propagating Bose-condensed atoms has been recently achieved with a chip-limited sensing area of $\sim 1500\mu m^2$ [21].

The interfering path of the device reported here consists of a reciprocal set of two-turn loops (four turns in total). The overall length of the path is $53cm$ and the total enclosed area A^* (if unwound) is $225cm^2$, $\sim$22 times larger than the typical areas used for single-loop devices employed in the past [22] and 3 orders of magnitude larger than typical areas used in state-of-the-art atom gyroscopes [14, 23]. We have configured the device in reciprocal geometry so that most of this area is cancelled by the counter-winding loops (with $\vec{A}_1 + \vec{A}_2 \approx 0$ in Fig 1(b)), leaving an effective area $|\vec{A}_3| \sim 6.6cm^2$ by design. A heater (R) and a thermal sink (S) are installed in the device so that $\Delta\phi_h$ can be induced in one half of the reciprocal set of loops. This acts as an adjustable differential phase shifter. The total phase shift in the device is $\Delta\phi_{ext} = \Delta\phi_s + \Delta\phi_h + \Delta\phi_b$, where $\Delta\phi_b$ represents any other constant current bias in the loop.

We first demonstrate the reciprocal principle by measuring the Earth's rotation $\vec{\Omega}_E$ through the Sagnac phase shift $\Delta\phi_s$ with $\Delta\phi_h = 0$. The area vectors $\vec{A}_1$, $\vec{A}_2$, and $\vec{A}_3$ all point horizontally in the laboratory. Thus we can vary the product $\vec{\Omega}_E \cdot \vec{A}$ by reorienting the interferometer about a vertical axis in the lab frame. Fig 2 shows the result of this reorientation for several different temperatures. We plot the overall mass current oscillation amplitude vs. $\Delta\phi_s/2\pi$. It is clear that interference persists even in this multiple-turn geometry. Here $\vec{\Omega}_E \cdot \vec{A} = \Omega_E A cos\theta_L sin\Theta$, where Θ is the direction of $\vec{A}$ with respect to an east-west line, and $\theta_L \approx 42.3^\circ$ is the latitude of Cambridge. Excellent fits (solid lines) yield $\vec{A} = (7.1cm^2)\hat{A}_3 \approx \vec{A}_3$. The fact that we observe the Sagnac effect with an associated area of A_3 rather than the total area A^* shows that the phase shift in A_1 is indeed cancelled by that in A_2, confirming a successful implementation of the reciprocal path configuration.

For interferometry that does not require the Sagnac effect (such as Berry's phase investigations and gauge-field rotation of polarized Bose condensates [20, 24]), the reciprocal configuration can be used to maintain the interfering path length while removing some of the unwanted area that inevitably couples the device to the environmental noise. In that configuration, one (or both) of the reciprocal sections can be used for probing particular physical interactions of interest. To test such a differential mode of operation, we have driven superfluid current in one half of the reciprocal set of the interfering path as depicted in Fig 1(b). The observed oscillation amplitude vs. $\Delta\phi_h/2\pi$ is plotted in Fig 3(a). In this case, the Sagnac contribution $\Delta\phi_s$ to the overall phase shift can be viewed as an unwanted perturbation, which is significantly reduced by the cancelled area as $\Delta\phi_s \propto A$. Fits (solid lines) yield $l/\sigma = 5.7 \times 10^4$ [1/m]. The design values of $l = 0.19m$ and $\sigma = 3.6 \times 10^{-6}m^2$ give $l/\sigma = 5.3 \times 10^4$ [1/m]. This result complements the Sagnac result shown in Fig 2 and provides further evidence that the matter-based interferometry is possible with superfluid in a multiple-turn reciprocal path.

Laser interferometers overcome their intrinsic sensitivity disadvantage by the use of large sensing area made possible by better beamsplitters and high finesse mirrors. Atom interferometers stay competitive with their intrinsically high sensitivity although their sensing areas remain relatively small, currently limited by the lack of better atom optics

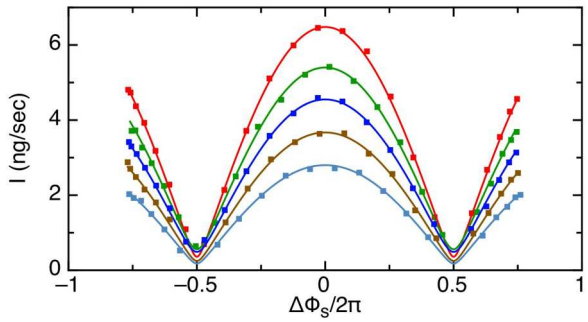

FIG. 2. Measured mass current oscillation amplitude vs. Sagnac phase shift induced by Earth's rotation. $T_\lambda - T$=6, 5, 4, 3, and 2mK (from the top).

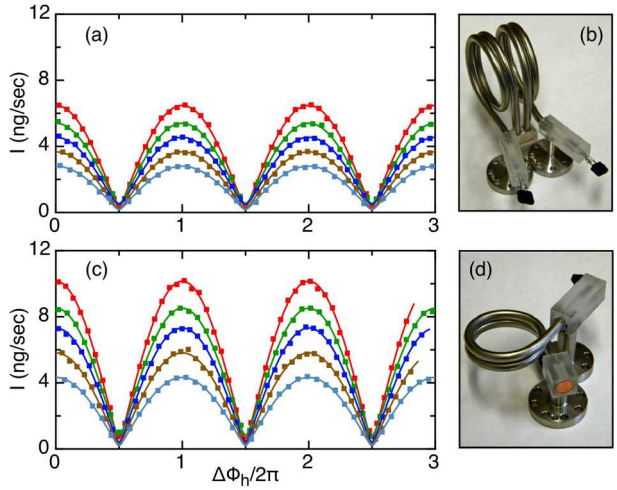

FIG. 3. (a) Measured mass current oscillation amplitude vs. $\Delta\phi_h/2\pi$. (b) 4-turn interfering path. (c) Same measurement as (a) for a 2-turn interferometer. (d) 2-turn interfering path. For figures (a) and (c), $T_\lambda - T$=6, 5, 4, 3, and 2mK (from the top).

and, more importantly, dispersion from waveguide imperfections amplified by betatron oscillations [8, 25]. Although a lack of such dispersive effects in a superfluid system makes it attempting to wind more loops, we show that the sensing area cannot be scaled up indefinitely. In Fig 3(c), we plot the measured oscillation amplitude vs. $\Delta\phi_h$ for a shorter loop with two turns (See Fig 3(d) vs.(b)). The total path length for this apparatus is $28cm$, $\sim 50\%$ of the four-turn configuration. The same arrays of channels are used and channel dimensions are verified with normal flow measurements above T_λ. We find that the modulation depth is shallower for the device with a longer path. To explain this behavior, we turn to the effect of increasing hydrodynamic inductance associated with the interfering path.

In the field of superconducting magnetometry [19], a separate pickup loop, having a much larger flux capture area than the 'bare' SQUID, is typically utilized and coupled to the SQUID inductance via a flux transformer. Such a scheme, made possible by the mutual inductance between the primary and secondary coils, allows an appropriate impedance matching required for the significant increase of sensing area. Unlike the charged superconducting counterpart, no coupling exists between two loops of neutral superfluid placed nearby. Therefore, in the superfluid quantum interference device, the pickup element needs to be the superfluid loop consisting of two weak link junctions (equivalent to a bare SQUID). This uncoupled circuitry of superfluid interferometers makes the hydrodynamic impedance matching an issue as the interfering path is made longer. The configuration resembles uncoupled SQUIDs often employed in SQUID-based microscopes and gradiometric miniature susceptometers for the study of small magnetic samples [19, 26].

Writing the fluid kinetic energy in terms of the mass current $E = LI^2/2$, the superfluid hydrodynamic inductance can be identified as $L = (\hbar/m_4)(dI/d\Delta\phi)^{-1}$ [27]. For superfluid in a weak link junction, $I = I_0 sin\Delta\phi$ leads to kinetic inductance of the weak link (called the Josephson inductance) $L_J = \hbar/(m_4 I_0)$ at $\Delta\phi = 0$. In contrast, for superfluid flowing through the rest of the interfering path made of simple tube of length l and cross-sectional area σ,

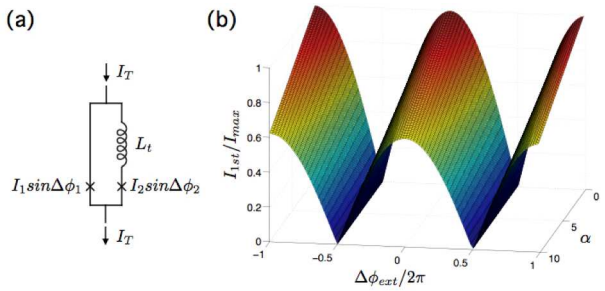

FIG. 4. (a) Electrical analogue of the apparatus. (b) Simulated interference patterns vs. $\Delta\phi_{ext}/2\pi$ for different α's.

the inductance $L_t = l/(\rho_s \sigma)$.

We model our interferometry device as an electrical circuit represented in Fig 4(a). The total current passing through the device is $I_T = I_1 sin\Delta\phi_1 + I_2 sin\Delta\phi_2$, where $\Delta\phi_1$ and $\Delta\phi_2$ are the phase drops across the two junctions. The hydrodynamic inductance L_t associated with the long interfering path also gives rise to a phase drop $(m_4/\hbar)L_t I_2 sin\Delta\phi_2$. The phase integral condition [18] $\oint \vec{\nabla}\phi \cdot d\vec{l} = 0$ applied to this circuit yields $(\Delta\phi_1 - \Delta\phi_2) - \alpha sin\Delta\phi_2 + \Delta\phi_{ext} = 0$. Here $\alpha \equiv L_t/L_J$ is the ratio of the inductance associated with the interfering path to the Josephson inductance. We note that α is related to the modulation parameter $\beta_L = 2LI_0/\Phi_0$ (often used in the analysis of SQUID dynamics) by $\alpha = \pi\beta_L$, with the magnetic flux quantum Φ_0 replaced by the superfluid circulation quantum $\kappa_4 = h/m_4$ [18]. The interferometer behavior is now described by $I_T(\theta)$ where $\theta \equiv (\Delta\phi_1 + \Delta\phi_2 + \alpha sin\Delta\phi_2)/2$.

The Fourier transform of the current-phase relation can be written as $I_T(\theta)/I_{max} = a_0/2 + \sum_{n=1}^{\infty}[a_n cos(n\theta) + b_n sin(n\theta)]$, where $a_n = (1/\pi)\int_{-\pi}^{\pi} I_T(\theta')cos(n\theta')d\theta'$ and $b_n = (1/\pi)\int_{-\pi}^{\pi} I_T(\theta')sin(n\theta')d\theta'$. We define the normalized amplitude of the first harmonic $I_{1st}/I_{max} = \sqrt{a_1^2 + b_1^2}$ and plot it as a function of α in Fig 4(b). It is apparent that increasing the interfering path length (and hence α) leads to shallower modulation depth, as evidenced in this experiment. Configured as a gyroscope, although one achieves significant rotational sensitivity gain from the increased area as $\delta\Omega \propto \delta\phi_s/A$, higher series-inductance compromises some of this gain. We emphasize again that this arises from the device's dependence on nonlinear collective effects and its inherent similarity to a bare dc-SQUID rather than conventional atom and optical interferometers.

For the 4-turn reciprocal device and the 2-turn device discussed here, we estimate $\alpha \sim 9$ and 4 respectively [28]. Increasing the cross-sectional area of the interfering path should decrease L_t and hence α, allowing one to harness the maximum sensitivity gain with large-area interferometers. Increased compressibility of the fluid arising from larger fluid volume should be addressed in such configurations. Alternatively, one may take advantage of the similarity to dc-SQUIDs and employ the so-called "multi-loop dc-SQUID" configuration where several large pickup loops are connected in parallel across the same junctions to reduce the loop inductance while giving an effective area that equals that of a single loop [19].

Josephson phenomena have been observed in Bose-Einstein condensates with a weak link [29, 30]. The first closed-loop atom circuit has been recently realized [31], paving a way to a BEC version of a dc-SQUID. As in the case of a superfluid device described above, a BEC quantum interference device is expected to produce nontrivial gauge potentials by rotation, making it a promising candidate for a sensitive inertial sensor. Multiple-turn and reciprocal concepts are applicable to such systems, and equivalent impedance matching should be considered.

For the device with counter-wound sensing loops discussed here, the rotational sensitivity (suppressed by design) is found to be $\approx 4 \times 10^{-7} rad/sec/\sqrt{Hz}$ at $T_\lambda - T = 6mK$. If the interfering path is unwound or wound only in one direction, the sensitivity would then increase by a factor of A^*/A_3, giving a projected resolution of $\approx 1 \times 10^{-8} rad/sec/\sqrt{Hz}$.

In conclusion, we have demonstrated a proof-of-principle superfluid ^{4}He quantum interference device with a multiple-turn reciprocal path. With considerations to the effect of increasing hydrodynamic inductance associated with a longer interfering path, this approach should play an important role in developing a new generation of force sensors suited for various applications such as rotation sensing. Our findings also reveal several fascinating similarities and dissimilarities between superfluid interferometers and atom and optical equivalents as well as superconducting quantum interference devices.

The authors thank D. Rogers for machining, S. Bevis for infrastructure support, R. Packard and D. Pekker for discussion, and J. VanDelden for nanofabrication work. This research was supported by the Rowland Institute at Harvard University.

[1] G. E. Stedman, Rep. Prog. Phys. **60**, 615 (1997).
[2] M. Kasevich, Science **298**, 1363 (2002).
[3] F. Riehle *et al.*, Phys. Rev. Lett. **67**, 177 (1991).
[4] M. Cerdonio *et al.*, Gen. Rel. Grav. **20**, 83 (1988).
[5] J. F. Clauser, Physica B **151**, 262 (1988).
[6] C. H. Rowe *et al.*, Appl. Opt. **38**, 2516 (1999).
[7] V. Vali and R. W. Shorthill, Appl. Opt. **15**, 1099 (1976).
[8] K. W. Murch *et al.*, Phys. Rev. Lett. **96**, 013202 (2006).
[9] S. Wu *et al.*, Phys. Rev. Lett. **99**, 173201 (2007).
[10] B. D. Josephson, Phys. Lett. **1**, 251 (1962).
[11] K. Sukhatme *et al.*, Nature **411**, 280 (2001).
[12] E. Hoskinson *et al.*, Nature **433**, 376 (2005).
[13] S. A. Werner *et al.*, Phys. Rev. Lett. **42**, 1103 (1979).
[14] T. L. Gustavson *et al.*, Phys. Rev. Lett. **78**, 2046 (1997).
[15] A. Lenef *et al.*, Phys. Rev. Lett. **78**, 760 (1997).
[16] O. Avenel *et al.*, JLTP **135**, 745 (2004).
[17] F. Hasselbach and M. Nicklaus, Phys. Rev. A **48**, 143 (1993).
[18] D. R. Tilley and J. Tilley, *Superfluidity and Superconductivity* (Institute of Physics, Bristol, 1990).
[19] J. Clarke and A. I. Braginski, *The SQUID Handbook: Fundamentals and Technology of SQUIDs and SQUID systems* (Wiley-VCH, Weinheim, 2004).
[20] E. B. Sonin, Phys. Rev. Lett. **102**, 106407 (2009).
[21] G. B. Jo *et al.*, Phys. Rev. Lett. **98**, 030407 (2007).
[22] E. Hoskinson *et al.*, Phys. Rev. B **74**, 100509R (2006).
[23] T. L. Gustavson *et al.*, Class. Quantum Grav. **17**, 2385 (2000).
[24] A. V. Balatsky *et al.*, Phys. Rev. Lett. **93**, 266801 (2004).
[25] A. E. Leanhardt *et al.*, Phys. Rev. Lett. **89**, 040401 (2002).
[26] A. Barone and G. Paterno, *Physics and Applications of the Josephson Effect* (John Wiley & Sons, New York, 1982).
[27] K. K. Likharev, *Dynamics of Josephson Junctions and Circuits* (Academic Press, New York, 1986).
[28] These α's provide upper limits as ρ_s can be suppressed considerably in nano-channels. See I. Rudnick *et al.*, Phys. Rev. Lett. **19**, 488 (1967).
[29] M. Albiez *et al.*, Phys. Rev. Lett. **95**, 010402 (2005).
[30] S. Levy *et al.*, Nature **449**, 579 (2007).
[31] A. Ramanathan *et al.*, Phys. Rev. Lett. **106**, 130401 (2011).